

# Synthesis of vanadium doped ZnO nanoparticles by sol–gel method and its characterization

J. El Ghoul<sup>1,2</sup>

Received: 12 September 2015 / Accepted: 30 October 2015 / Published online: 6 November 2015  
© Springer Science+Business Media New York 2015

**Abstract** The synthesis of  $\text{Zn}_{1-x}\text{V}_x\text{O}$  nanoparticles by a sol–gel processing technique for  $x$  ranging from 0 to 0.08 was reported in this work. In our approach, the water for hydrolysis was slowly released by esterification reaction followed by a supercritical drying in ethyl alcohol. The obtained nanopowder was characterized by various techniques. The results of X-ray diffraction, X-ray photoelectron spectroscopy and transmission electron microscope indicated that the V ion was incorporated in to the crystal lattices of wurtzite ZnO nanoparticles. Photoluminescence (PL) spectra consist of a very wide and strong emission band located in the visible range where the intensity and energy position depend on the PL measurement temperature. Magnetic measurements at room temperature showed a diamagnetic for undoped ZnO and ferromagnetic behavior after doping with vanadium. The mechanism of nanoparticles formation and the comparison with recent results are discussed.

## 1 Introduction

In recent years, semiconductor nanoparticles have attracted great interest. This is stimulated mainly by physical probe into low-dimensional systems and potential applications

for this class of materials. They always exhibit novel optical, electrical, and mechanical properties due to quantum confinement effects compared with their bulk counterparts, and thus can be applied in many areas, including luminescent devices, solar cells, chemical sensors, and biological labeling and diagnostics.

Zinc oxide is an excellent n-type semiconductor with a wide band gap of 3.37 eV and a large exciton binding energy of 60 meV [1, 2]. For these reasons, ZnO is used in a wide variety of applications, including opto-electronic devices [3, 4], catalysis [5], light-emitting diodes (LEDs) [6], thermoelectric devices [7], varistors [8, 9], flat panel displays [9] and surface acoustic wave devices [10]. Recent theoretical predictions [11, 12] proposed transition metal (TM)-doped ZnO as one of the most promising candidates for room temperature ferromagnetism (RTFM). Additionally, the excellent optical transparency of ZnO and the possibility of band gap engineering through TM doping strongly encourages the exploration of the magneto-optical properties of the TM-doped ZnO system which might lead to the development of novel magneto-optoelectronic devices [13–15].

A promising way to produce magnetic functionality in existing semiconductors is to dope them with magnetically active transition metals. Electronic structure calculations by Karamat and Mera [11, 12] led to two self-consistent solutions for the TM ions incorporated in dilute magnetic semiconductors (DMSs): (1) a ferromagnetic (FM) state stabilized by the double exchange interaction between the moments via the hopping of itinerant d electrons between the TM neighbours, and (2) a spin glass (SG) state of randomly oriented magnetic moments dominated by anti-ferromagnetic (AF) superexchange interactions. The stability of the FM state over the SG state depends on the difference between the total energies of the two states, and

✉ J. El Ghoul  
ghoultn@yahoo.fr; jaber.elghoul@fsg.rnu.tn

<sup>1</sup> Department of Physics, College of Sciences, Al Imam Mohammad Ibn Saud University (IMSIU), Riyadh 11623, Saudi Arabia

<sup>2</sup> Laboratory of Physics of Materials and Nanomaterials Applied at Environment (LaPhyMNE), Faculty of Sciences in Gabès, Gabès University, 6072 Gabès, Tunisia

this directly corresponds to the ordering temperature  $T_c$ . Among the II-VI compounds, ZnO is the most favourable system for RTFM since it shows a positive energy difference for V, Cr, Fe, Co or Ni doping and negative energy difference only for Mn doping. This indicates that V, Cr, Fe, Co or Ni-doped ZnO might directly stabilize an FM state while Mn-doped ZnO might form an SG state. Karamat and Mera [11, 12] have further shown that the magnetic properties of TM-doped ZnO can be varied systematically by changing the carrier concentration. Previous studies have obviously demonstrated that the physical and chemical properties of the synthesized  $Zn_{1-x}V_xO$  samples are strongly sensitive to its preparative conditions [2, 16]. Over the past few years, much effort has been made to investigate wet chemical methods for the synthesis of metal-ion-doped ZnO nanostructures, including the sol-gel method [17, 18] and various hydrothermal methods [19, 20].

Motivated by these reasons, we report in this paper a new approach to obtain such powders based on hydrolysis of zinc acetate in methanol followed by supercritical drying in ethanol using modified sol-gel process. The effect of vanadium as TM doping element on structural, optical and magnetic properties of the powder is investigated for different concentrations.

## 2 Experimental details

Vanadium-doped ZnO nanocrystals were prepared by the sol-gel method using 16 g of zinc acetate dehydrate as precursor in a 112 ml of methanol. After magnetic stirring at room temperature, the appropriate amount of ammonium metavanadate was added, and the solution was placed in an autoclave and dried under supercritical conditions of ethyl alcohol.

X-ray diffraction (XRD) patterns of vanadium doped zinc oxide nanopowder were carried out by a Bruker D5005 diffractometer, using  $CuK\alpha$  radiation ( $\lambda = 1.5418 \text{ \AA}$ ). The dopant content and the chemical bonding states of Vanadium ions in the  $Zn_{1-x}V_xO$  nanocrystallites were determined using XPS (PHI-5702). The synthesized products were also characterized using a JEM-200CX transmission electron microscopy (TEM). The specimens for TEM were prepared by putting the as-grown products in EtOH and immersing them in an ultrasonic bath for 15 min, then dropping a few drops of the resulting suspension containing the synthesized materials onto TEM grid. UV-VIS DRS were recorded on Shimadzu UV3101PC Visible spectrophotometer in the wavelength range of 200–1500 nm. BaSO<sub>4</sub> was used as a standard for these measurements. For PL measurements, a 450-W Xenon lamp was used as an excitation source. The

magnetic response of  $Zn_{1-x}V_xO$  nanoparticles was detected by sensible measurements of the magnetization as a function of the field (0 to  $\pm 65$  kOe) using a commercial superconducting quantum interference device (SQUID) magnetometer (Quantum Design, MPMS XL).

## 3 Results and discussion

Figure 1 shows the XRD patterns of  $Zn_{1-x}V_xO$  ( $0.0 \leq x \leq 0.08$ ) samples after treatment temperature at 500 °C. In the case of undoped ZnO, we noticed the appearance of nine pronounced diffraction peaks at  $2\theta = 31.82^\circ, 34.61^\circ, 36.36^\circ, 47.55^\circ, 56.73^\circ, 62.88^\circ, 66.34^\circ, 68.08^\circ$  and  $69.19^\circ$  which can be attributed to the (100), (002), (101), (102) (110), (103), (200), (112) and (201) planes of ZnO, respectively [21, 22]. After doping of ZnO with vanadium and thermal treatment, in addition to the peaks corresponding to ZnO, four secondary additional phases were detected which can be attributed to  $V_2O_3$  and  $Zn_3(VO_4)$  (JCPDS Card 37-1485) [21]. Due to the small size of the crystallites in the aerogel, the diffraction lines are broadened and are further found to depend on the Miller indices of the corresponding sets of crystal planes. For our samples, the (002) diffraction line is always narrower than the (101) line and the latter is narrower than the (100) line. This indicated an asymmetry in the crystallite shape. The average grain size can be calculated using the Debye-Scherrer equation [23]:

$$G = 0.9\lambda/B\cos\theta_B \quad (1)$$

where  $\lambda$  is the X-ray wavelength ( $1.5418 \text{ \AA}$ ),  $\theta_B$  is the maximum of the Bragg diffraction peak and  $B$  is the linewidth at half maximum. After a correction for the

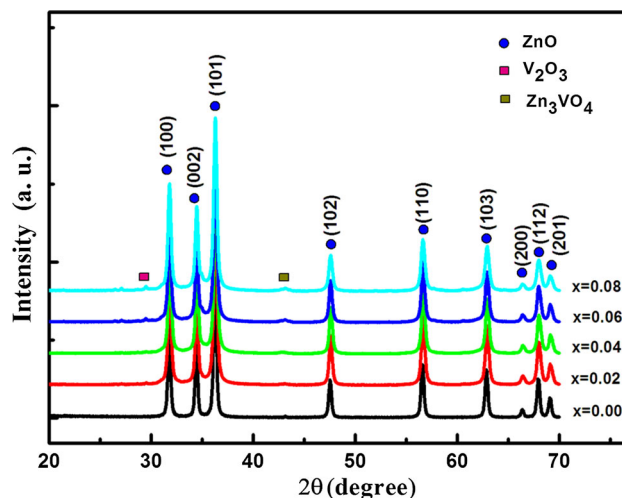


**Fig. 1** XRD patterns of  $Zn_{1-x}V_xO$  nanoparticles for various vanadium doping levels

instrumental broadening, an average value of crystallites is found to be 18–30 nm.

The lattice constants are  $a = 3.195 \text{ \AA}$  and  $c = 5.217 \text{ \AA}$  for the  $\text{Zn}_{0.94}\text{V}_{0.06}\text{O}$  sample. The ratio of  $a/c$  of  $\text{Zn}_{0.94}\text{V}_{0.06}\text{O}$  is 0.612, which is slightly smaller than that of pure ZnO (0.624) which might be due to the smaller size of vanadium ion [24]. The obtained values of the lattice parameters and grain size of  $\text{Zn}_{1-x}\text{V}_x\text{O}$  samples are given in Table 1. The shift in peaks implies systematically incorporation of V ions for the Zn ions in the lattice without changing its wurtzite structure consistent with previously reported observations [25]. It is desirable in DMS that the doping atom must substitute the ions of the host lattice. In ZnO system, dopants of 5+ oxidation state mostly substitute the  $\text{Zn}^{2+}$  ions in the lattice due to charge matching. In case of vanadium doping, the ionic radius of  $\text{V}^{5+}$  (0.72 Å) ion is quite bigger than the  $\text{Zn}^{2+}$  (0.60 Å) ion. If  $\text{V}^{5+}$  ion substitutes  $\text{Zn}^{2+}$  ion in the lattice then the change in the lattice parameters is expected due to ionic radii mismatch which has also been reported by others [26].

To confirm further the chemical bonding states of V ions in the doped ZnO, XPS measurements were carried out the V doped ZnO sample. The XPS spectrum presented in Fig. 2 shows that the indexed peaks are corresponding to those of C, V, O and Zn. The asymmetric peak was observed in the O-1s region (530–533 eV). This peak has been attributed to the  $\text{O}^{2-}$  ions in the normal wurtzite structure of ZnO powder [27] and  $\text{O}^{2-}$  ions in the oxygen-deficient regions within the ZnO matrix [28, 29], respectively. The high resolution scans of the XPS spectra of V 2p have been shown in the inset of Fig. 2. Based on the Gauss fitting, the peaks of V 2p<sub>3/2</sub> are detected at 517.4 eV for the sample. The position of the peak is different from those of Vanadium metal,  $\text{V}^{2+}$ ,  $\text{V}^{3+}$  and  $\text{V}^{4+}$  located at 512.3, 513.7, 515.3 and 515.8 eV respectively. In contrast, the position of this peak is very near to the peak position of V 2p<sub>3/2</sub> (517.2 eV) in  $\text{V}_2\text{O}_5$  [30, 31]. It suggests that the V dopants are incorporated into the ZnO lattice as  $\text{V}^{5+}$  ions. The NPs displays a doublet at about 1021 and 1044 eV

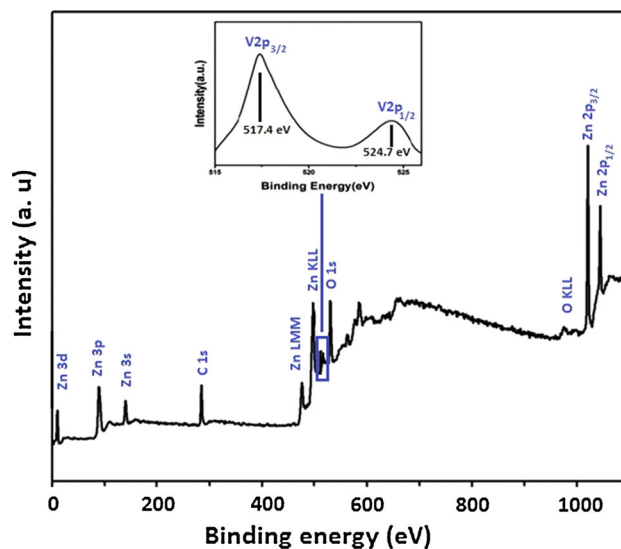


Fig. 2 XPS spectra of V-doped ZnO

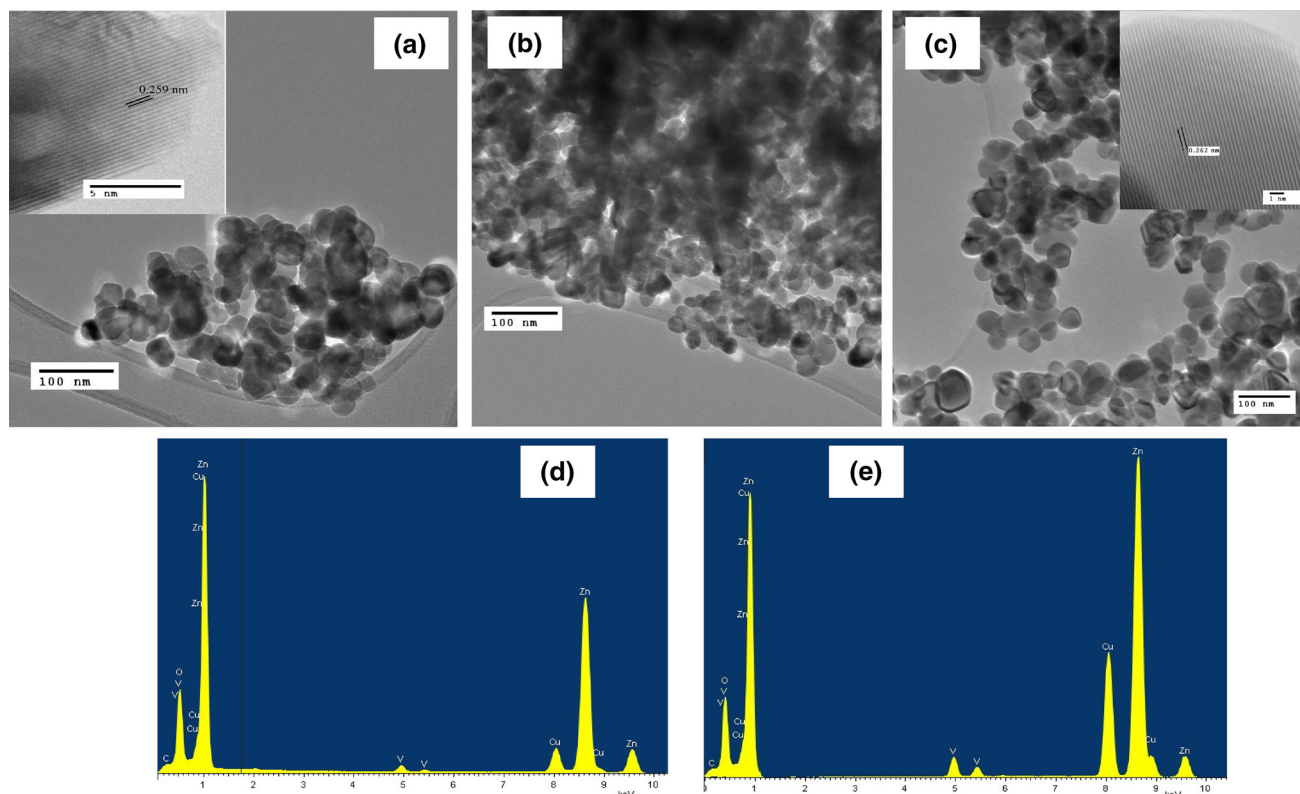
(vertical reference lines), corresponding to the  $\text{Zn-}2p_{3/2}$  and  $2p_{1/2}$  core levels [32]. The first peak is attributed to  $\text{Zn}^{2+}$  ions in the oxygen-deficient ZnO matrix [28]. Moreover, the all of Zn 2p<sub>3/2</sub> XPS peaks are sharp. Thus, it can be confirmed, that Zn element exists mainly in the form of  $\text{Zn}^{2+}$  on the samples surfaces [29].

Figure 3 shows the TEM images of representative  $\text{Zn}_{1-x}\text{V}_x\text{O}$  ( $x = 0.0, 0.04$  and  $0.08$ ) samples, the HRTEM image of ZnO and EDX analyzes of doped samples. The morphologies of all the samples are found to be nearly spherical in nature with the diameters ranging from 19 to 30 nm. It clearly shows that the average particle size of these samples is nanoscale and it decreases as  $x$  increases, which is consistent with the results of X-ray diffraction. The HRTEM images clearly showed that the measured distances between the planes of the fringes is 0.259 and 0.261 nm (Fig. 3a, b), respectively, which is corresponding to the (002) planes of the wurtzite ZnO, confirming the growth of the parameter  $c$  calculated by XRD (Table 1). The EDX spectra of the doped samples showed signals directly related to dopant. Zn and O appeared as the main components with low levels of V (Fig. 3b, c). These measurements showed an increase in the relative intensities of the V peaks with increasing  $x$ , confirming the progressive incorporation of V. This ensures the uniform distribution of the doped V ions as expected in the chemical synthesis process employed in this work (Fig. 3d, e).

The UV–VIS diffuse absorption spectra of undoped ZnO and vanadium doped ZnO are shown in Fig. 4. It is found that the absorption of all ZnO:V are higher than undoped ZnO. The absorption coefficient  $\alpha$  is related to the optical energy band gap  $E_g$  for high photon energies as [22]:

**Table 1** Lattice parameter values, the crystallite size of the nanopowder sample calculated from the XRD patterns and the energy gap of V-doped ZnO nanopowders estimated from the spectrum  $(\alpha h\nu)^2$  curve towards the  $(h\nu)$

V (at.%)	d (Å)	c (Å)	D (nm)	$E_g$ (eV)
0	2.604	5.208	29.8	3.188
2	2.606	5.212	26.2	3.185
4	2.607	5.214	24.7	3.181
6	2.608	5.217	22.2	3.170
8	2.609	5.218	21.3	3.162



**Fig. 3** HR-TEM images and EDX analysis of ZnO (a),  $Zn_{0.96}V_{0.04}O$  (b) and  $Zn_{0.92}V_{0.08}O$  (c) nanoparticles

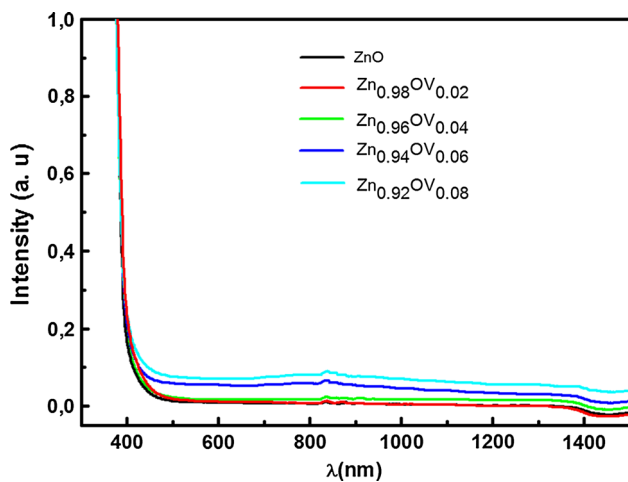


**Fig. 4** UV-vis-IR absorption spectrum of  $Zn_{1-x}V_xO$  nanoparticles for various vanadium doping levels

$$\alpha(h\nu) = C(h\nu - E_g)^{\frac{1}{2}} \quad (2)$$

where  $C$  is a constant for direct transition, and  $h\nu$  is the energy of the incident photon. The plot of  $(\alpha h\nu)^2$  against  $(h\nu)$  shows a linear dependence. This means that ZnO are direct transition type semiconductor. The band gap energy ( $E_g$ ) is determined by extrapolating the linear part of the

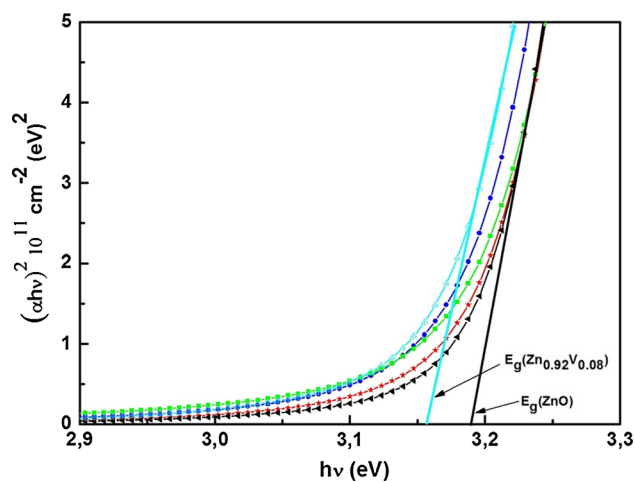


**Fig. 5** Plots of  $(\alpha h\nu)^2$  versus photon energy  $h\nu$  of  $Zn_{1-x}V_xO$  nanoparticles for various vanadium doping levels

spectrum  $(\alpha h\nu)^2$  curve towards the  $(h\nu)$  axis in Fig. 5. The obtained value for the band gap energies of the  $Zn_{1-x}V_xO$  varies between 3.19 and 3.15 eV (refer Table 1), corresponding to the violet-blue region of the electromagnetic spectrum [33]. It is found that the optical band gap of samples (inset of Fig. 5) shows a decrease with the increase of doping concentration. Since  $E_g$  of vanadium oxide

(2.5 eV) is lower than that of ZnO, it is reasonable to expect that the  $E_g$  decrease with vanadium doping.

Figure 6 shows the PL spectra of the ZnO:V nanopowder measured at different temperatures and undoped zinc oxide at 78 K. In the case of undoped sample, we note the appearance of a luminescence peak at 385 nm attributed to the band gap of ZnO. In the case of V-doped ZnO, the PL spectra consist of a very wide and strong emission band located in the visible range from green-yellow-red where the intensity and energy position depends on the PL measurement temperature. The intensity of the PL band increases with decreasing PL measurement temperature. However, it appears a blue shift. It is well known that introducing impurity into the semiconductor can change its structural and optical properties. The origins of the emission bands in ZnO, are yet highly controversial and many attributions have been proposed [34]. It has been suggested that the green emission is associated to oxygen deficiency, while the orange–red emission is associated to oxygen excess [35]. For the origin of green emission, a number of hypotheses have been proposed, such as singly ionized oxygen vacancy [35], centre [36], oxygen antisite [37], and zinc vacancy  $V_{Zn}$  [38]. On the other hand, yellow and red emissions were attributed to different initial states (conduction band and shallow donors) [39]. The red emission was also attributed to the interstitial zinc  $Zn_i$  [40]. Yellow emission is commonly attributed to interstitial oxygen defects  $O_i$  [41]. Vanheusden et al. [36] observed a green emission in ZnO and attributed it to the recombination between singly charged oxygen vacancy and photoexcited hole. We suggest that this luminescence band is attributed to the contribution of complex of oxygen vacancy and zinc interstitial  $V_O-Zn$  and oxygen vacancy simply loaded  $V_O^+$  [18]. Furthermore, the PLE spectrum detected at 550 nm are given in (Fig. 7.) shows a very

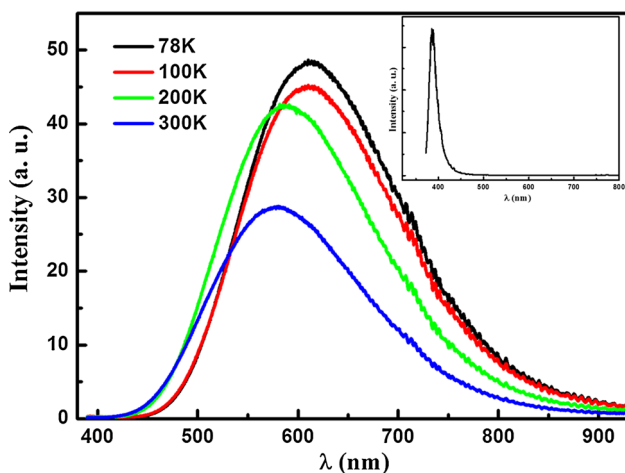


**Fig. 6** PL spectra of the ZnO:V nanopowder at different temperatures. The inset showing PL spectra of undoped ZnO

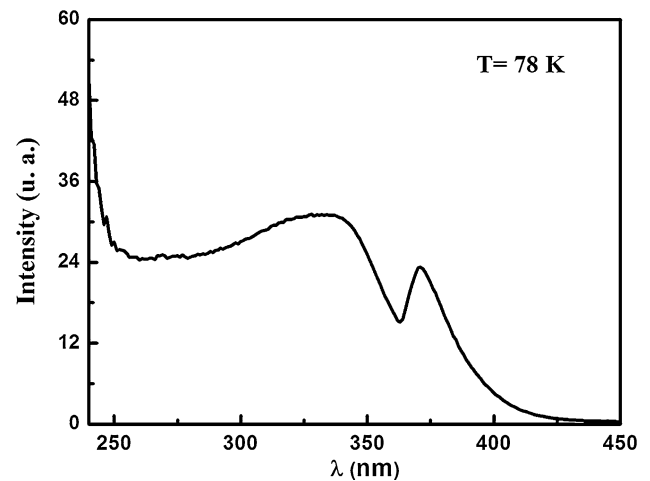


**Fig. 7** PLE spectra of the ZnO:V nanopowder

weak excitation band at 250–350 nm and a very sharp and strong peak at 371 nm, this position correspond to the band gap of ZnO.

Figure 8 shows the dependence of magnetization with the applied magnetic field ( $M-H$  curves) of  $Zn_{1-x}V_xO$  ( $x = 0.0, 0.04$  and  $0.08$ ) measured at room temperature (300 K). We observe a diamagnetic behavior in the case of undoped ZnO and the ferromagnetic to others samples. The hysteresis loops for this sample present with the coercivity ( $H_c$ ) values 294.8 and 789.2 Oe, and the remnant magnetization ( $M_r$ ) values  $1.99 \cdot 10^{-3}$  and  $3.59 \cdot 10^{-3}$  emu/g. At present due to controversial results there seems to be no single theory that can explain the ferromagnetism in all oxide DMS's. A defect mediated ferromagnetism model based on bound magnetic polaron (BMP) theory has been predicted theoretically [42] and confirmed experimentally [43] to play a crucial role in activation of ferromagnetism

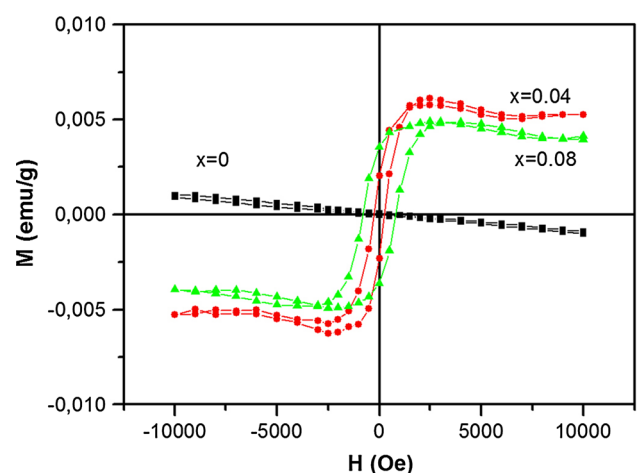


**Fig. 8**  $M-H$  curves of  $Zn_{1-x}V_xO$  ( $x = 0.00, 0.04$  and  $0.08$ ) at room temperature

in oxide DMS's. All the magnetic ions within the polaronic radius interact ferromagnetically and for a sufficient large numbers of bound magnetic polarons long range ferromagnetic order is established. The secondary phase and metal clusters sometimes contribute to the ferromagnetism for ZnO-based diluted magnetic semiconductors [44]. The formation of secondary phase such as V-metal clusters or V-oxide precipitates should be considered such a possible origin of ferromagnetism in V-doped ZnO samples. But in our case, the origin of room-temperature magnetism could not be derived from any impurity phase because the VO<sub>2</sub> is non-magnetic and V<sub>2</sub>O<sub>3</sub>, V<sub>6</sub>O<sub>13</sub> and ZnV<sub>2</sub>O<sub>4</sub> are antiferromagnetic [45]. Among V metal and oxides, only V metal clusters are ferromagnetic at room temperature, whereas the formation of V clusters is unlikely because our samples were calcined in aerobic atmosphere. In addition, the corresponding signal of V element was observed by XRD and XPS as mentioned above. Consequently they can be the sources of ferromagnetism in our samples.

#### 4 Conclusion

Nanocrystalline Zn<sub>1-x</sub>V<sub>x</sub>O powders have been synthesized by a simple sol-gel method. The synthesis protocol is based on a slow hydrolysis of the precursor using an esterification reaction, followed by a supercritical drying in EtOH. XRD results indicated that all the synthesized undoped and V-doped ZnO samples had the wurtzite structure and no secondary phases was detected which indicated that Co ions substituted for Zn ions. FETEM results revealed that the prepared V doped ZnO nanoparticles are nearly spherical in shape with particle size <30 nm, which is in good agreement with the size obtained from XRD. The band gap energy of the samples decreases from 3.19 eV (undoped ZnO) to 3.16 eV (8 at.% V:ZnO), indicating that V doping has a crucial influence on the energy band structure of ZnO. PL spectra of the nanopowder show strong luminescence band. From the analysis of these results, it can be concluded that the vanadium related defect complexes are responsible of this luminescence band. In addition, the samples show a transition from diamagnetic to the ferromagnetic behavior after doping probably due to the incorporation of V in ZnO matrix.

#### References

1. L. Yan, C.K. Ong, X.S. Rao, *J. Appl. Phys.* **96**, 508–511 (2004)
2. L. El Mir, J. El Ghoul, S. Alaya, M. Ben Salem, C. Barthou, H.J. von Bardeleben, *Phys. B* **403**, 1770–1774 (2008)
3. R. Razali, A. Khorsand Zak, W.H.A. Majid, M. Darroudi, *Ceram. Int.* **37**, 3657–3663 (2011)
4. P. Sharma, K. Sreenivas, K.V. Rao, *J. Appl. Phys.* **93**, 3963–3970 (2003)
5. M.L. Curri, R. Comparelli, P.D. Cozzoli, G. Mascolo, A. Agostiano, *Mater. Sci. Eng. C* **23**, 285–289 (2003)
6. H. Kim, J.S. Horwitz, W.H. Kim, A.J. Makinen, Z.H. Kafafi, D.B. Chrisey, *Thin Solid Films* **420**, 539–543 (2002)
7. A.I. Abutaha, S.R. Sarath Kumar, H.N. Alshareef, *Appl. Phys. Lett.* **102**, 053507–053511 (2013)
8. J.V. Bellinia, M.R. Morelli, R.H.G.A. Kiminami, *Mater. Lett.* **57**, 3775–3778 (2003)
9. M. Chen, Z.L. Pei, C. Sun, J. Gong, R.F. Huang, L.S. Wen, *Mater. Sci. Eng. B* **85**, 212 (2001)
10. A. Furukawa, N. Ogasawara, R. Yokozawa, T. Tokunaga, *Jpn. J. Appl. Phys.* **47**, 8799–8801 (2008)
11. S. Karamat, R.S. Rawat, T.L. Tan, P. Lee, R. Chen, H.D. Sun, W. Zhou, *Appl. Phys. A* **101**, 717–722 (2010)
12. J. Mera, C. Córdoba, J. Benavidez, O. Paredes, J. Doria, A. Gómez, C. Sanchez, C. Paucar, O. Morán, *J. Mater. Sci.* **45**, 5398–5405 (2010)
13. A. Nakamura, J. Ishihara, S. Shigemori, K. Yamamoto, T. Aoki, H. Gotoh, J. Temmyo, *Jpn. J. Appl. Phys.* **44**, 7267–7270 (2005)
14. N. Lebedeva, P. Kuivalainen, *J. Appl. Phys.* **93**, 9845–9864 (2003)
15. J. El Ghoul, M. Kraini, L. El Mir, *J. Mater. Sci.: Mater. Electron.* **26**, 2555–2562 (2015)
16. J. Guo, W. Zhou, P. Xing, P. Yu, Q. Song, P. Wu, *Solid State Commun.* **152**, 924–928 (2012)
17. J.H. Yang, L.Y. Zhao, X. Ding, L.L. Yang, Y.J. Zhang, Y.X. Wang, H.L. Liu, *Mater. Sci. Eng. B* **162**, 143–146 (2009)
18. M.E. Mercurio, A.W. Carbonari, M.R. Cordeiro, R.N. Saxena, L.Z. D'Agostino, *J. Magn. Magn. Mater.* **322**, 1195–1197 (2010)
19. X.L. Zhang, R. Qiao, J.C. Kim, Y.S. Kang, *Cryst. Growth Des.* **8**, 2609–2613 (2008)
20. A. Singhal, S.N. Achary, J. Manjanna, S. Chatterjee, P. Ayyub, A.K. Tyagi, *J. Phys. Chem. C* **114**, 3422–3430 (2010)
21. J. El Ghoul, C. Barthou, L. El Mir, *Superlattices Microstruct.* **51**, 942–951 (2012)
22. J. El Ghoul, C. Barthou, L. El Mir, *Phys. E* **44**, 1910–1915 (2012)
23. J. El Ghoul, M. Kraini, O.M. Lemine, L. El Mir, *J. Mater. Sci.: Mater. Electron.* **26**, 2614–2621 (2015)
24. X.S. Wang, Z.C. Wu, J.F. Webb, Z.G. Liu, *Appl. Phys. A* **77**, 561–565 (2003)
25. S. Ramachandran, A. Tiwari, J. Narayan, J.T. Prater, *Appl. Phys. Lett.* **87**, 172502–172504 (2005)
26. E. Chikoidze, Y. Dumont, F. Jomard, D. Ballutaud, P. Galtier, O. Gorochov, D. Ferrand, *J. Appl. Phys.* **97**(10), D327–D329 (2005)
27. J. Haber, J. Stoch, L. Ungier, *J. Electron Spectrosc. Relat. Phenom.* **9**, 459–467 (1976)
28. S.Y. Huang, Q.J. Cheng, S. Xu, D.Y. Wei, H.P. Zhou, J.D. Long, I. Levchenko, K. Ostrikov, *J. Appl. Phys.* **111**, 036101–036103 (2012)
29. J. Liqiang, W. Dejun, W. Baiqi, L. Shudan, X. Baifu, F. Honggang, S. Jiazhong, *J. Mol. Catal. A: Chem.* **244**, 193–200 (2006)
30. G.A. Sawatzky, D. Post, *Phys. Rev. B* **20**, 1546–1555 (1979)
31. G. Silversmit, D. Depla, H. Poelman, G.B. Marin, R.D. Gryse, *J. Electron Spectrosc. Relat. Phenom.* **135**, 167–175 (2004)
32. O. Lupan, G.A. Emelchenko, V.V. Ursaki, G. Chai, A.N. Redkin, A.N. Gruzintsev, I.M. Tiginyanu, L. Chow, L.K. Ono, B. Roldan Cuenya, H. Heinrich, E.E. Yakimov, *Mater. Res. Bull.* **45**, 1026–1032 (2010)
33. S. Senthilkumaar, K. Rajendran, S. Banerjee, T.K. Chini, V. Sengodan, *J. Mater. Sci. Semicond. Process.* **11**, 6–12 (2008)
34. B.J. Jin, S. Im, S.Y. Lee, *Thin Solid Films* **366**, 107–110 (2000)
35. A. Teke, U. Ozgur, S. Dogan, X. Gu, H. Morkoc, B. Nemeth, J. Mause, H.O. Everitt, *Phys. Rev. B* **70**, 195207–195210 (2004)
36. K. Vanheusden, C.H. Seager, W.L. Warren, D.R. Tallant, J.A. Voigt, *Appl. Phys. Lett.* **68**, 403–405 (1996)

37. A. Van Dijken, E.A. Meulenkaamp, D. Vanmakelbergh, A. Meijerink, *J. Phys. Chem. B* **104**, 1715–1723 (2000)
38. B. Lin, Z. Fu, Y. Jia, *Appl. Phys. Lett.* **79**, 943–945 (2001)
39. Q.X. Zhao, P. Klason, M. Willander, H.M. Zhong, W. Lu, J.H. Yang, *Appl. Phys. Lett.* **87**(2005), 211912–211921 (1913)
40. S.A. Studenikin, N. Golego, M. Cocivera, *J. Appl. Phys.* **84**, 2287–2294 (1998)
41. L. El Mir, A. Amlouk, C. Barthou, S. Alaya, *Phys. B* **388**, 412–417 (2007)
42. J.M.D. Coey, M. Venkatesan, C.B. Fitzgerald, *Nat. Mater.* **4**, 173–179 (2005)
43. K.A. Griffin, A.B. Pakhomov, C.M. Wang, S.M. Heald, K.M. Krishnan, *Phys. Rev. Lett.* **22**, 157204–157208 (2005)
44. H. Liu, X. Cheng, H. Liu, J. Yang, Y. Liu, X. Liu, M. Gao, M. Wei, X. Zhang, Y. Jiang, *Phys. E* **47**, 1–5 (2013)
45. N. Tahir, S.T. Hussain, M. Usman, S.K. Hasanain, A. Mumtaz, *Appl. Surf. Sci.* **255**, 8506–8510 (2009)